MADRID
inter.noise 2019
June 16 - 19
NOISE CONTROL FOR A BETTER ENVIRONMENT

Investigation on the Use of a Passive Nonlinear Absorber for the Reduction of Vibration in the Mast of a Floating Offshore Wind Turbine

Antonio Cillis[1]
Ecole Centrale de Lyon
36 Avenue Guy de Collongue, 69134 Écully, France

Emmanuelle Sarrouy[2], **Pierre-Olivier Mattei**[3]
Aix Marseille Univ, CNRS, Centrale Marseille, LMA
4 Impasse Nikola Tesla, 13013 Marseille, France

Riccardo Mariani[4], **Thomas Choisnet**[5]
Ideol
375 avenue du Mistral, 13600 La-Ciotat, France

ABSTRACT

Floating Offshore Wind Turbines (FOWT's) are subjected to different types of dynamic loads such as environmental loads (wave and wind), aero-structure interaction loads and mechanical loads (inertial and controller effects). These loads induce vibrations in the WT mast that are transmitted in the floating foundation and mooring lines, increasing the overall ultimate loads and fatigue cycling.

In this paper the potentiality of a passive nonlinear mechanical system for the reduction of WT mast vibrations is studied. This kind of absorber called Nonlinear Energy Sink (NES) is based on the energy pumping phenomenon.

The feasibility and efficiency of the absorber is first demonstrated by means of a simplified full-scale numerical model composed of two degrees of freedom, one for the WT mast (first bending mode) and one for NES.

Then, an equivalent reduced scale model is considered and analyzed by numerical simulations and experiments.

The study is concluded with the sizing of an optimized absorber for the full-scale system. Some sensitivity analyses considering variations of the mast structural characteristics (stiffness and structural damping) are performed to investigate the NES efficiency limits, confirming the performances of the NES: reduction of vibratory level around 8-10 dB over a large range of loads.

Keywords: Wind Turbines (WT), Energy pumping, Nonlinear Energy Sink (NES)
I-INCE Classification of Subject Number: 54
http://i-ince.org/files/data/classification.pdf

[1]antonio.cillis@auditeur.ec-lyon.fr,
[2]emmanuelle.sarrouy@centrale-marseille.fr, [3]mattei@lma.cnrs-mrs.fr
[4]riccardo.mariani@ideol-offshore.com, [5]thomas.choisnet@ideol-offshore.com

1. INTRODUCTION

Despite active work along the years, reducing noise and vibration remains a very attractive research topic because it allows improved fatigue resistance with a consequent reduction in maintenance costs and environmental impact. Many active and passive devices have been developed to improve the vibroacoustics behavior of mechanical systems.

Horizontal axis WT's can be subject to vibrations because of the combination of random wind loads and rotor spinning. WT drivetrain vibrations are countered in many cases by integrating active torque dampers in the power converters. The most common ways of reducing tower vibrations are by using pendulum dampers, sand-boxes or by barring certain rotor spinning rates of turns. An alternate to these usual vibration control measures is investigated in this paper, based on a generic 10 MW three blade horizontal axis WT.

1.1. Dynamics of floating offshore wind turbine

Wind turbine (WT) structural dynamics is characterized by high modal density in a rather narrow low frequency range. The results of FE modal analysis performed by the software Nastran on the WT considered for this study (DTU 10 MW) in onshore condition (cantilever mast bottom), are summarized in Table 1. The first ten modes have natural frequencies concentrated between 0.47 and 1.78 Hz. Modes 1 and 2 correspond essentially to the bending of the mast (mast dominated modes), mode 3, 4, 7, 9 and 10 are related to the bending of blades (rotor dominated modes) and mode 5, 6 and 8 are essentially rotor dominated but strongly coupled with the bending of the mast.

mode No.	nat. freq. [Hz]	description	mode No.	nat. freq. [Hz]	Description
1	0.47	1st bending mast X	6	0.99	1st bending all blades + mast Y
2	0.48	1st bending mast Y	7	1.02	1st bending bottom blades Y
3	0.61	1st bending bottom blades X	8	1.04	1st bending top blade + mast Y
4	0.62	1st bending all blades X	9	1.71	2nd bending bottom blades X
5	0.66	1st bending all blades + mast X	10	1.78	2nd bending all blades X

Table 1. Results of FE modal analysi of WT in onshore condition.

For sake of conciseness only the mode shape of the mode 1 and 5 are depicted in Figure 1**Erreur ! Source du renvoi introuvable.**. They correspond to the lower frequency modes present in the dynamic response of the WT mast when it is excited in X direction (corresponding to the rotor axis direction), as shown in Figure 2, representing the power spectral density (PSD) of WT mast free response to an initial condition in terms of mast top elastic deflection. The response is calculated for two different WT (boundary) conditions: onshore (cantilever mast bottom, in red line), and fixed on Ideol floating foundation (blue line). For the onshore condition, by comparing with results presented in Table 1, it is possible to identify a first peak at 0.47 Hz corresponding to the mode 1 and a second peak at 0.66 Hz corresponding to the mode 5. For the floating condition the natural frequencies of these two modes are shifted toward higher frequencies (0.58 Hz and 0.74 Hz, respectively) and it is possible to observe the appearance of an additional peak (peak #3) around 0.065 Hz, associated to the platform rigid body pitch mode that is partially coupled with the mast bending deformation.

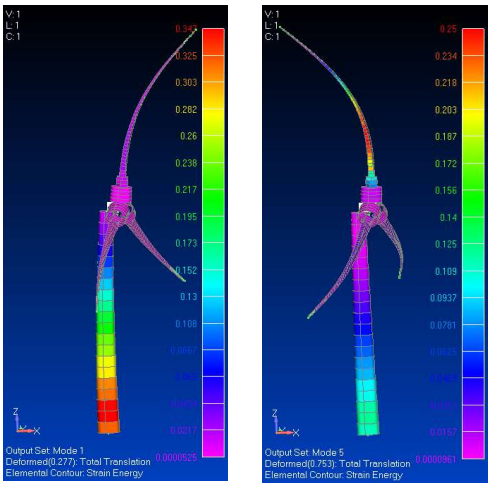

Figure 1. Shape of WT mode 1 (left) and mode 5 (right).

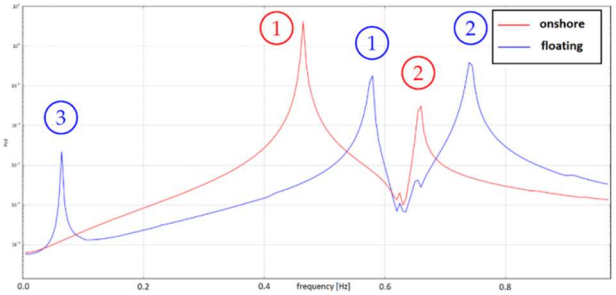

Figure 2; PSD [m²/Hz] of free response in terms of mast top elastic deformation in X direction for two WT conditions: onshore (red line) and floating (blue line).

The dynamic nature of loads applied on a FOWT is caused by a combination of natural and design factors. Wave excitation causes rigid body motions of the floater that carries the turbine. Given the low frequency range of wave excitation (see Figure 3 below) no structural modes are excited, and power variations are kept within acceptable limits by the controller of the wind turbine [5].

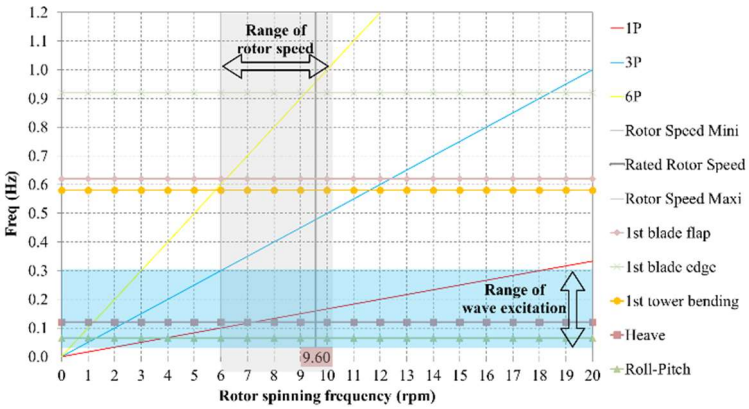

Figure 3. Campbell diagram of the FOWT.

WT's operate in the lower layer of the atmosphere, which features small-scale turbulence, variations of the wind speed with altitude and low frequency wind direction and speed changes. The natural wind field combined with the features of the WT causes most structural excitation.

Rotor imbalance causes excitation at the rotor spinning frequency (1P on Figure 3 above) that can be removed by weight balancing. The wind gradient and mast-blades aerodynamic interaction are the main source of loads at the blades passing frequency (3P). Low frequency wind direction changes are compensated by yawing the WT, but the turbine is never perfectly aligned with the wind. This combined with the wind gradient causes loads at 2 times the blades passing frequency (6P). Although the tower and blades feature resonance frequencies away from these rotational excitations, tower

vibration still takes place. It is a consequence of transient loads such as blades shading in the wake of the tower, vortex shedding along the tower, etc.

1.2. Energy pumping and NES

To mitigate structural vibration, the Frahm absorber, consisting of a mass-spring-damper system, tuned to the frequency of vibration to eliminate is very efficient but has a limited frequency range of effectiveness [1] and a significant increase of system mass. Passive non-linear Energy Pumping (EP) is a way to overcome such limitations [2]. The simplest case requires consideration of a linear mechanical system connected to a secondary oscillator having a strongly nonlinear stiffness (typically a cubic one). This attachment is usually termed as Non-linear Energy Sink (NES). This kind of non-linearity corresponds to a resonance of the NES that varies with the amplitude of excitation. This enables a passive nonlinear energy transfer that is realized through resonance capture at high energy value. Passive nonlinear energy transfer from the primary system to the NES occurs under resonance condition once the NES amplitude rises above a certain threshold; reverse energy flow from the NES to the primary system is prevented because of resonance escape due to the energy decrease induced by dissipation

To date a wide variety of NESs have been proposed and tested [2]. A recent theoretical and numerical work [3,4] showed that a bi-stable non-linear oscillator manifests significant advantages with respect to energy pumping efficiency. Using this principle, we have developed a non-linear bi-stable NES that provides improved robustness in frequency and range over existing passive devices by lowering the excitation threshold. This NES is based on a buckled plate with length l_N, height h_N and thickness e_N. This plate supports a concentrated mass M_P at its mid-length. The whole apparatus, depicted in Figure 4, is maintained and attached to the structure by a rigid support with mass M_S.

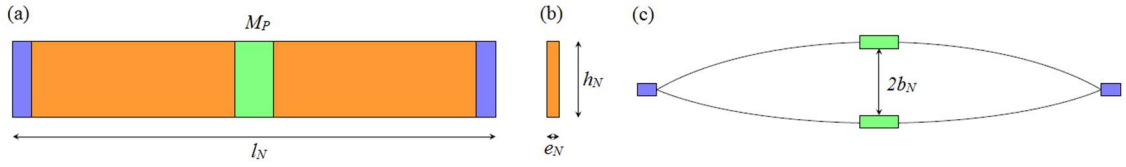

Figure 4. Bistable NES sketch. (a) Lateral view (b) Plate cross-section dimensions (c) Top view of buckled plate stable positions.

2. MODELLING AND SIMULATIONS

In order to have fast computations, simplified models are used for simulations. Hence, the next sections present first the studied WT and results of preliminary simulations for the characterization of main WT dynamic loads; then, the reduced WT model and the associated NES model equations are provided before showing results for a full-scale model and a reduced (experimental) model.

2.1. Wind turbine

The WT considered in this study is the DTU 10 MW, a numerical reference WT developed by the Technical University of Denmark for academic and R&D activity scope [5]. The main characteristics of this WT are listed in Table 2.

Rated power	10 MW	Hub height	119.0 m
Cut-in wind speed	4 m/s	Minimum rotor speed	6.0 rpm
Cut-out wind speed	25 m/s	Maximum rotor speed	9.6 rpm
Rated wind speed	11.4 m/s	Rotor-Nacelle Assembly (RNA) mass	674 t
Number of blades	3	Mast mass	892.5 t
Rotor diameter	178.3 m		

Table 2. Main characteristics of WT DTU 10 MW.

Some preliminary simulations were performed for the characterization of WT dynamic loads by using FAST, an open source code developed by National Renewable Energy Laboratory (NREL) to simulate the aero-hydro-servo-elastic behavior of WT's in onshore, offshore and floating offshore conditions. The aerodynamic load transmitted to the top of mast were calculated varying the mean wind speed v in the range from 4 to 25 m/s (WT cut-in and cut-out wind speed, respectively). This load results essentially in a harmonic component F_{3P} at 3P frequency ($f_{3P}=3f_{1P}$, with f_{1P} WT rotation frequency), superimposed to a mean load F_0.

(1) $$F(t,v) = F_0(v) + F_{3P}(v)cos(2\pi f_{3P}t) + \cdots$$

Figure 5 presents mean load F_0, amplitude of 3P load F_{3P} and variation of 3P excitation frequency f_{3P} as a function of wind speed v. It is possible to observe as the WT rotation speed (and thus the f_{3P}) and F_0 reach its maximum for v around the WT rated speed (11.4 m/s), whereas, for v larger than 11.4 m/s, the rotation speed is maintained constant and F_0 reduced for the effect of controller, resulting in a constant electrical power (10 MW).

This analysis permits to quantify the order of magnitude of the main dynamic load acting on the WT (F_{3P}), information necessary for the design and optimization of the NES.

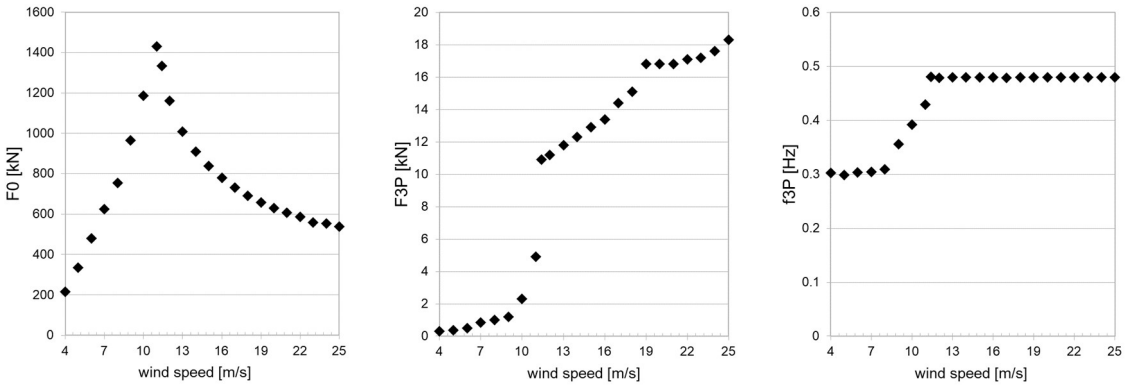

Figure 5. Characterization of WT dynamic load (FAST simulations): mean load, amplitude of 3P component load and 3P frequency as function of wind speed.

2.2. Wind turbine with NES model

The main dynamic load acting on a WT (3P) could have a strong impact especially on excitation of the 1st WT mast bending mode. Hence, a simple model for whole WT is built considering only 1 dof (degree of freedom). To this end, the WT geometry is first simplified: the mast is represented as a beam with length h_p and square section (inside and outside lengths denoted b_1 and b_2 respectively) and the RNA at its top end is

reduced to a concentrated mass M_T undergoing a harmonic force $F(t)=A\cos(\omega t)$, as depicted in Figure 6.

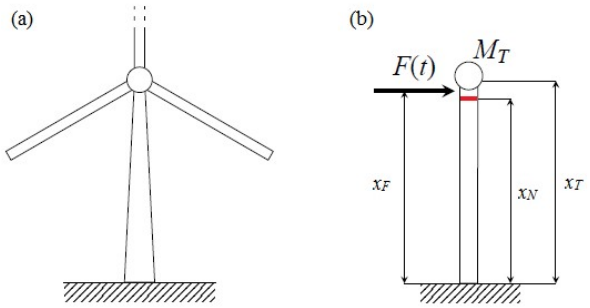

Figure 6. Reduced WT model. (a) Original geometry; (b) Simplified model including the NES (red line).

The lateral deflection $w(x,t)$ along the beam is then governed by the following equation (assuming an Euler-Bernoulli model):

$$(2) \quad EI\frac{\partial^4 w}{\partial x^4} + \left(\rho S + M_T\delta_{x_T}(x) + M_N\delta_{x_N}(x)\right)\frac{\partial^2 w}{\partial t^2} = \delta_{x_F}(x)A\cos(\omega t)\ (t)$$

where E is the beam material Young modulus, ρ is its density, $S=b_2^2-b_1^2$ the beam cross-section area and $I=(b_2^4-b_1^4)/12$ its second moment of area, M_N is the total mass of the NES apparatus and δ_x denotes the Dirac distribution at point x. Beam dimensions b_1 and b_2 were chosen so that the total mass is equal to total mast mass and that the second moment of area of the beam is equal to the one of the mast at middle height $h_p/2$.

The second step to obtain the final beam model is to reduce the displacement field w to be proportional to the first eigenshape of the beam alone, $\phi(x)$: $w(x,t) = \phi(x)u(t)$. When introducing damping μ_B, Equation (2) becomes:

$$(3) \quad m_B\,\ddot{u}+\mu_B\,\dot{u}+k_B u = \phi(x_F)A\cos(\omega t)$$

with $m_B=\rho S+M_T\,\phi^2(x_T)+M_N\,\phi^2(x_N)$ the dynamic mass and $k_B = \int_0^{h_T} EI\frac{\partial^4\phi}{\partial x^4}\phi\,dx$ the dynamic stiffness.

After a few transformations and assumptions [4], the NES behavior is described by:

$$(4) \quad m_N\,\ddot{q} + \mu_N\,\dot{q} + k_N F_{nl}(q) = 0$$

where m_N, μ_N and $k_N=(2\pi f_N)^2$ are the dynamic mass, damping and stiffness respectively. $m_N = (3/8)\,\rho_N S_N l_N + M_p$; μ_N and k_N are identified experimentally.

Coupling both structures gives:

$$(5) \quad \begin{cases} m_B\,\ddot{u}+\mu_B\,\dot{u}+k_B u - \mu_N(\dot{q}-\phi(x_N)\dot{u}) - k_N F_{nl}(q-\phi(x_N)u) = \phi(x_F)A\cos(\omega t) \\ m_N\,\ddot{q} + \mu_N(\,\dot{q}-\phi(x_N)\dot{u}) + k_N F_{nl}(q-\phi(x_N)u) = 0 \end{cases}$$

2.3. Full scale model simulations

Model described in Equation (5) is simulated using a Mathematica code for various excitation frequencies ω and amplitudes A when considering the full scale model.

NES dimensions were chosen based on the NES studied in [4] with a ×70 scale factor. They were then manually adjusted to find a first satisfying results set. Numerical values used for these simulations are given in Table 3. An optimization process will be applied later to the NES parameters in Sec. 4.1.

Lengths and RNA mass				
$L=x_T$ = 94.3 m	x_F = 93.5 m	x_N = 93.5 m	M_T = 675000 kg	
Beam properties				
E = 210 GPa	ρ = 7800 kg.m^{-3}	b_1 = 7.448 m	b_2 = 7.529 m	$\mu_B = 2\times0.05(2\pi f_B)$
NES properties				
l_N = 7 m	b_N = 0.35 m	h_N = 0.35 m	e_N = 7 10^{-3} m	M_P = 1 300 kg
E_N = 200 GPa	ρ_N = 7800 kg.m^{-3}	f_N = 0.55 Hz	$\mu_N = 2\times0.025(2\pi f_N)$	M_S = 14 000 kg

Table 3. Numerical values for full scale model.

These values give a first eigenfrequency f_B = 0.477 Hz for the beam plus RNA mass alone which is very close to the real problem first eigenfrequency (0.47 Hz). NES first eigenfrequency is taken equal to 0.55 Hz that is higher than the structure one with a relatively small damping rate (2.5 %). The frequency response function (FRF) is displayed in Figure 7(a): as expected the NES becomes active when excitation amplitude is large enough and "cuts" the structure response amplitude for a wide range of frequencies. Figure 7(b) displays the ridge curves for simulations with and without the NES being active (its added mass is always considered): for each excitation amplitude, the maximum value of the structure response amplitude over the whole frequency range is displayed. As expected, the ratio structure response over excitation amplitudes is constant when the NES is inactive, hence, the model is linear. When the NES is active however, a reduction up to 9 dB is obtained which is very encouraging and justifies the rest of the study.

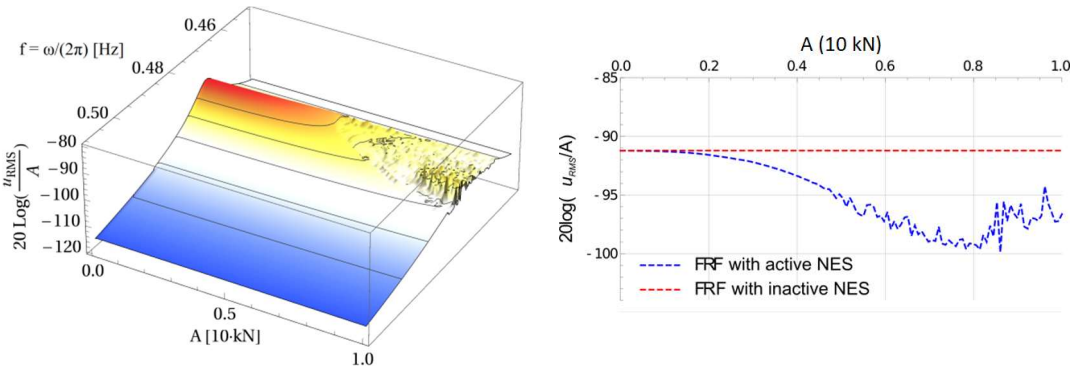

Figure 7. Full-scale model results. Left: FRF; Right ridge curves.

2.4. 1:100 scale model simulations

The next step will be to validate numerical results using an experimental set-up. As a full scale experimental campaign would be very costly to realize, a 1:100 scale model is first numerically designed before being experimentally tested.

Using a dimensionless abscissa $s=x/L$ and displacement $v(s,t)=w(sL,t)/L$, Equation (2) becomes, when divided by ρS and putting the NES mass aside:

$$(6) \qquad \frac{EI}{\rho SL^4}\frac{\partial^4 v}{\partial s^4} + \left(1 + \frac{M_T}{\rho SL}\delta_{s_T}(s)\right)\frac{\partial^2 v}{\partial t^2} = \delta_{s_F}(s)\frac{A}{\rho SL}\cos(\omega t) \;\; (t)$$

Now, to build a reduced model with ρ', E', I', L', S', M_T', M_N' and A' characteristics which preserves added mass ratio, first eigenfrequency and external loading one has to satisfy the following three equations:

(7) $\frac{M_T}{\rho SL} = \frac{M_T'}{\rho' S' L'}$, $\frac{EI}{\rho SL^4} = \frac{E'I'}{\rho' S' L'^4}$ and $\frac{A}{\rho SL} = \frac{A'}{\rho' S' L'}$

As the beam material is steel for both full scale and reduced scale models ($E=E'$, $\rho=\rho'$), one gets the properties for the equivalent beam with plain rectangular section (length L', width h' and thickness e') displayed in Table 4.

NES properties are chosen by starting from values described in [4] and modifying them until a satisfying result is obtained.

Lengths and RNA mass				
$L'=x_T'$ = 1.28 m	x_F' = 1.26 m	x_N' = 1.20 m	M_T' = 0.8 kg	
Beam properties				
E' = 210 GPa	ρ' = 7800 kg.m^{-3}	h' = 5 10^{-2} m	e' = 2 10^{-3} m	μ_B' = 2×0.05$(2\pi f_B)$	f_B^e = 1.135 Hz
NES properties				
l_N' = 0.102 m	b_N' = 0.6 10^{-3} m	h_N' = 0.01 m	e_N' = 0.2 10^{-3} m	M_P' = 12 10^{-3} kg
E_N' = 200 GPa	ρ_N' = 7800 kg.m^{-3}	f_N' = 0.54 Hz	μ_N'=2×0.026$(2\pi f_N)$	M_S' = 30 10^{-3} kg

Table 4. Numerical values for reduced (1:100) scale model.

Results obtained for this reduced scale model with values in **Erreur ! Source du renvoi introuvable.** are presented in Figure 8. This configuration provides a beam vibration amplitude reduction up to 11 dB.

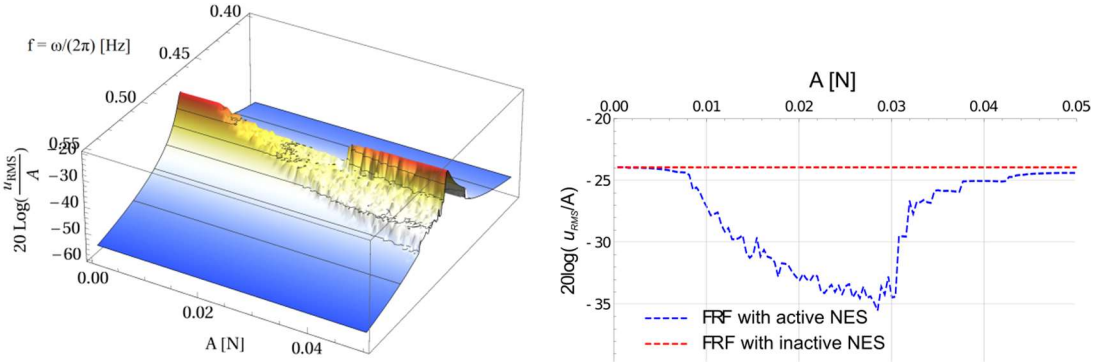

Figure 8. Reduced scale model result. Left: FRF; Right ridge curves.

3. EXPERIMENTAL VALIDATION

The objective of this section is to validate the promising results obtained numerically using an experimental set-up.

3.1. Experimental set-up

A beam with plain rectangular section similar to the one analyzed in Sec. 2.4 is used. Its real parameters are provided in Table 5 along with NES and other parameters. For instrumentation purpose, the beam is horizontal rather than vertical.

Figure 9 shows a photo as well as a sketch of the experimental set-up. An excitation is applied at the bottom of the beam using a type 4810 Brüel & Kjær shaker associated to a type 2706 Brüel & Kjær amplifier. Three laser displacements sensors (Keyence LK-G32, LK-G82 and LKG-152) monitor the excitation induced displacement u_F, an intermediate beam displacement u_B and the NES displacement u_N respectively. Finally,

a Polytec PSV-400 laser vibrometer driven by an OFV-400 controller measures the beam velocity v_B closer to the mass.

Lengths and RNA mass				
L^e = 1,3 m	x_T^e = 1.18 m	x_F^e = 1.26 m	x_N^e = 1.28 m	M_T^e = 0.802 kg
Beam properties				
E^e = 210 GPa	ρ^e = 7800 kg.m^{-3}	h^e = 3 10^{-2} m	e^e = 4 10^{-3} m	μ_B^e=2×0.008$(2\pi f_B)$	f_B^e = 1.135 Hz
NES properties				
l_N^e = 0.12 m	b_N^e = 2 10^{-3} m	h_N^e = 0.05 m	e_N^e = 0.5 10^{-3} m	M_P^e = 23 10^{-3} kg
E_N^e = 200 GPa	ρ_N^e = 7800 kg.m^{-3}	f_N^e = 4.25 Hz	μ_N^e=2×0.02$(2\pi f_N^e)$	M_S^e = 80 10^{-3} kg
Sensors locations				
x_{uF} = 0.078 m	x_{uB} = 0.512 m	x_{vB} = 0.945 m	x_{uN} = 1.352 m	

Table 5. Numerical values for experimental set-up

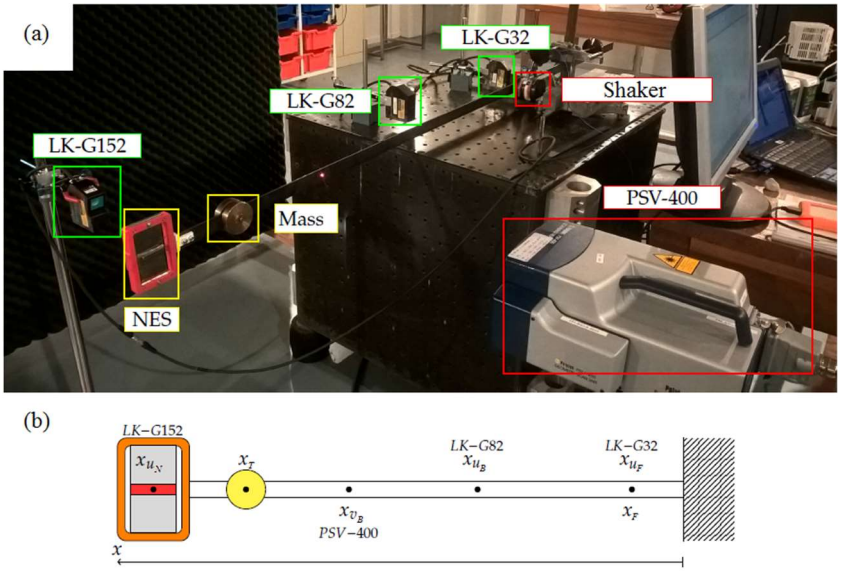

Figure 9. Experimental set-up: (a) photo; (b) sketch with important abscissa.

3.2. Results of the tests with white noise excitation

A first series of tests are run with white noise excitation with small amplitudes A so as to stay in the linear regime. From these tests, FRF (ratio u_B/A) are drawn. First, the configuration is as depicted in Figure 9 and the excitation amplifier is set to A = 0.1 V. This provides the beam dynamical properties f_B^e = 1.13 Hz and μ_B^e (as well as higher modes) but the NES first mode does not appear as can be seen on Figure 10(a). Then the beam is excited but without the turbine mass M_T and still very small excitation amplitudes (A = 0.025 V). Removing the mass M_T makes the beam eigenfrequencies higher and let the NES first mode appear (cf. Figure 10(b)). Hence, its dynamical properties f_N^e = 4.25 Hz and μ_N^e can be identified.

These first measures indicate that the NES first frequency is higher than expected (about 3 times the beam first mode).

From the previous series of measures (no RNA mass, white noise excitation), one can identify the experimental NES efficiency by fitting a 2 dofs FRF function using least mean square method to reproduce the first 2 visible modes of the beam. This lets

us draw the amplitude curves depicted in Figure 11. These curves show that the current NES has the ability to largely reduce mode 2 amplitude, especially when excitation amplitudes A are high but does not act on mode 1 in this configuration. The most noticeable feature showed in this case lies in the fact that the NES works well under random excitation while predictions are obtained only under harmonic forcing.

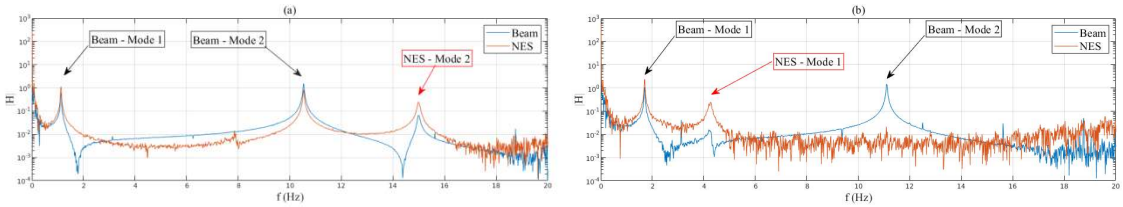

Figure 10. Experimental FRF for (a) complete structure and (b) structure without M_T.

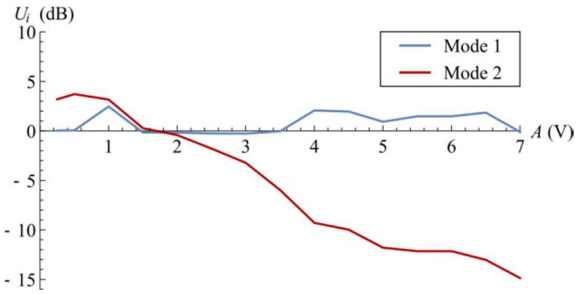

Figure 11. Modes amplitude for white noise excitation, no turbine mass.

3.3. Results of the tests with sinusoidal excitation

A second series of measures used a sinusoidal excitation at the structure resonance frequency f_B^e identified previously for different levels of excitation amplitude A. Sweeping a whole frequency range would have been too long as the whole system is very poorly damped, hence the transient regime can take several minutes to disappear. This series of experiments provides the last parameter of the reduced model which has not been identified yet: the gain γ between excitation amplifier input voltage and the effective applied force: A [N] = γ A [V]. This parameter is adjusted so as to have the NES becoming active for the same level of excitation; this happens for $\gamma = 3$ N.m^{-1}. The adjusted model simulations are then compared to experimental results in Figure 12(a).

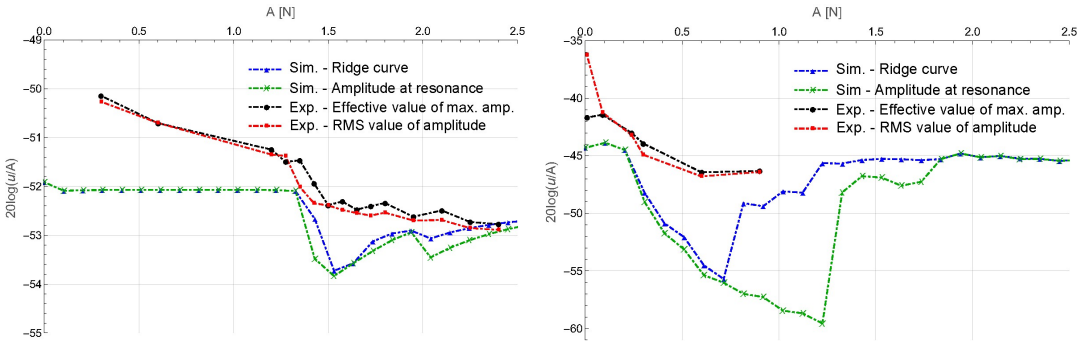

Figure 12. Left:Gain adjustment with turbine mass; Right: comparison of adjusted model simulations and experiments without turbine mass

The obtained adjusted model is then used for simulations without the turbine mass. These results are compared to experimental results described in Sec. 3.1 (cf. Figure

12(b)). The NES activation level is then correctly predicted which makes us confident for the model reliability. In both cases, simulation and experimental curves share the same profile even though the numerical model overestimates the amplitude reduction.

These results prove that this very simple model is able to qualitatively describe the real structure and can be used for a first full scale design while keeping computation times reasonable.

4. OPTIMIZATION OF THE NES AND SENSITIVITY STUDY

4.1. Optimal sizing of NES

The NES applied to the full-scale model described in Sec. 2.2 is manually tuned to obtain the best structure amplitude reduction over the widest excitation amplitude range. This study led to attenuation results presented in Figure 13 for the NES parameters given in Table 6 (structure parameters are still the ones in Table 3).

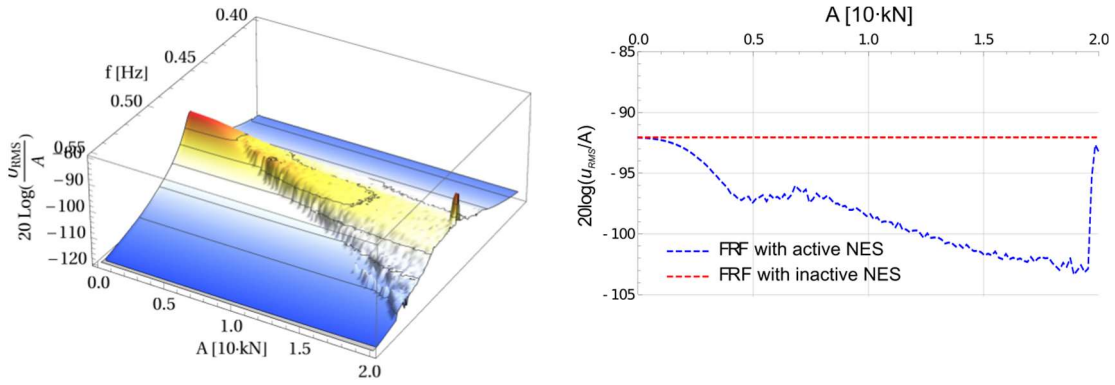

Figure 13. Optimized NES. Left: FRF; Right: Ridge curves

When the NES is active (for $A \geq 4$ kN), amplitude reduction is at least 5 dB and up to 11dB which is rather interesting.

NES properties				
l_N = 7 m	b_N = 0.07 m	h_N = 0.45 m	e_N = 45 10^{-3} m	M_P = 20 000 kg
E_N = 200 GPa	ρ_N = 7800 kg.m^{-3}	f_N = 0.64 Hz	μ_N =2×0.10$(2\pi f_N)$	M_S = 14 000 kg

Table 6. Numerical values for optimized NES.

The total mass of the NES is about 34 tons which is 2% of the RNA mass. This ratio lies in the classical range for absorbers. Decreasing the mass of the absorber usually decreases its efficiency.

4.2. Sensitivity analysis on structural parameters of the WT mast

This study ends with a sensitivity analysis to test the NES robustness to structure parameters variations. Both the structure stiffness and its damping modal rate were varied. Results are shown in Figure 14.

Considering rather large structure stiffness variations (±10% that is f_B = 0.45/0.47/0.50 Hz), the NES keeps limiting the response amplitude to a certain level. The stiffer the structure is the higher are the excitation levels for which the NES is active.

Increasing damping decreases NES efficiency as the structure itself tends to have lower response amplitudes. However, even though is it less efficient, it still has a visible

action for commonly damped structures (1% damping rate): 4 to 7 dB can be gained that is amplitude ratios from 0.63 to 0.45.

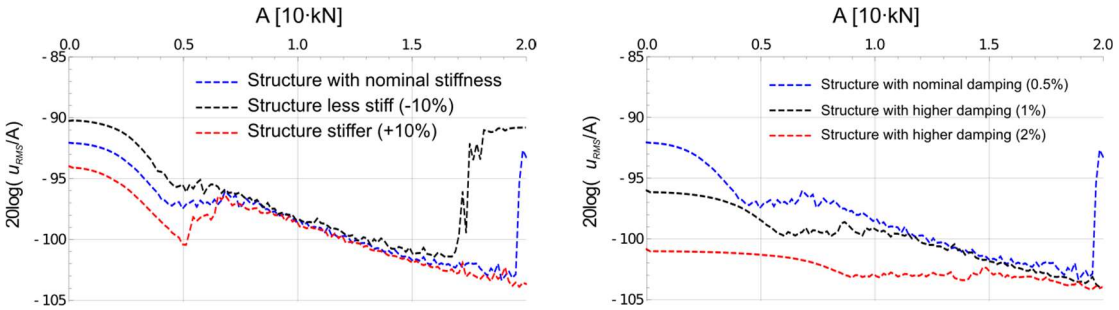

Figure 14. Sensitivity analysis: ridge curves. Left: stiffness; Right: damping

5. CONCLUSIONS

In this paper a 2 dof model was validated via experiments showing good qualitative agreement with lack of accurate amplitude reduction prediction. The experiment carried out on the reduced scale model has demonstrated the ability of the NES to reduce vibration amplitude of several modes.

The full-scale simplified numerical model of WT equipped with NES has shown the efficiency of the NES to reduce vibrations of the WT and its robustness with respect to the variation of structure properties.

In order to improve NES efficiency, a real constrained optimization algorithm on NES for full scale model has to be implemented.

For industrial application the feasibility of such a large and heavy structure should be tested in terms of mechanical resistance (overall constraints and fatigue) on a reduced scale WT.

6. REFERENCES

1. J.P. Den Hartog, *Mechanical Vibration*, McGraw-Hill, New York (1947).
2. A.F. Vakakis, O.V. Gendelman, L.A. Bergman, D.M. McFarland, G. Kerschen, Y.S. Lee, *Nonlinear Targeted Energy Transfer in Mechanical and Structural Systems (two volumes)*, Springer Verlag, Berlin (2008).
3. L.I. Manevitch, G. Sigalov, F. Romeo, L.A. Bergman, A. Vakakis, *Dynamics of a Linear Oscillator Coupled to a Bistable Light Attachment: Analytical Study,* ASME Journal of Applied Mechanics 81, 041011-1-9 (2014).
4. P.-O. Mattei, R. Ponçot, M. Pachebat, R. Côte, *Non-linear targeted energy transfer of two coupled cantilever beams coupled to a bistable light attachment*, Journal of Sound and Vibration, vol. 337, pp. 29-51 (2016).
5. C. Bak, F. Zahle, R. Bitsche, T. Kim, A. Yde, L.C. Henriksen, P.B. Andersen, A. Natarajan, M.H. Hansen, *Design and performance of a 10 MW wind turbine,* J. Wind Energy, to be accepted.
6. R. Buils Urbano, M. de Battista, A. Alexandre, E. Norton, Y. Percher, M. Favré, *Control retro-fit for the Floatgen floating wind turbine: from paper into reality*, FOWT Conference (2018).